Theoretical and Applied Fracture Mechanics 106 (2020) 102444

Contents lists available at ScienceDirect

Theoretical and Applied Fracture Mechanics

journal homepage: www.elsevier.com/locate/tafmec

A method for improving the crack resistance of aluminum alloy aircraft skin inspired by plant leaf

Lushen Wu[a], Teng Wang[a,b], Yun Hu[a,c,*], Jiaming Liu[a], Minjie Song[a]

[a] School of Mechatronics Engineering, Nanchang University, Nanchang 330031, China
[b] School of Aerospace Engineering, Xiamen University, Xiamen 361102, China
[c] Department of Mechanical Engineering, Imperial College London, London SW7 2AZ, UK

ARTICLE INFO

Keywords:
Plant leaf
Bio-inspired structure
Aircraft skin
Crack extension
Stress intensity factor

ABSTRACT

Aircraft skins are likely to experience cracks and fracture failure due to the combined action of shear, bending, and torsional load. Inspired by the crack resistance exhibited by plant leaf, a method is proposed to improve the crack resistance of aluminum alloy aircraft skin. The characteristic parameters of main and secondary leaf veins are extracted by image edge detection and analysis methods. According to a constructed collection of self-similar fractal sets, a bio-inspired residual stress field with fractal characteristics extracted from leaf veins is applied to specimens ahead of crack tip by using laser peening. The effects of fractal parameters on crack retardation are analyzed using interaction integral. The results show that the stress intensity factor ahead of crack tip is reduced by applying a bio-inspired residual stress field, whereas the plastic zone area ahead of crack tip is enlarged. The correlation between these two trends reveals the mechanism of stress intensity decrease after the introduction of bio-inspired residual stress field. The optimal crack retardation effect is achieved at a fractal angle of 55°, at which the residual fatigue life is increased by up to 203.0%. Compared with square-shaped laser peening, full-coverage laser peening, square criss-cross pattern method, and single-edge notched tensile (SENT) specimen repair method, the proposed method achieves the longest residual fatigue life, which is almost three times that of the square-shaped laser peening method. Therefore, this theoretical study presents a potential method for improving the crack resistance of aluminum alloy aircraft skin.

1. Introduction

Aircraft skin accounts for more than 50% of the total weight of the entire aircraft, thus, integral connection technology has been gradually used instead of assembly connection technology to connect aircraft and skeleton. This greatly reduces the number of aircraft parts and the weight of fuselage [1]. However, once cracks appear in aircraft skin, it is very difficult to retard crack propagation due to the lack of rivet holes, which are used to arrest crack development in integral panel structures. Consequently, the damage tolerance ability of aircraft skin will begin to deteriorate.

In order to improve the damage tolerance ability of aircraft skin, research has predominantly focused on selective reinforcement technology to improve crack growth resistance. Mechanical connection repair and gluing repair are two common selective reinforcement methods. Zhang et al. [2] analyzed the shear performance and failure modes of bolt connectors and found that the shear bearing capacity of the bolt connectors increased as bolt diameter, tensile strength, and concrete strength increase. Moreover, Guo et al. [3] reported that the bolt arrangement patterns and structural forms are closely related to the failure mode and bearing capacity of bolt connectors. It should also be noted that, if bolt connectors are used to prevent crack growth, cracks will occur at the hole-edge due to stress concentration or contact interaction between hole and bolt [4–6]. In addition, the use of fasteners can lead to an increase in the weight of panels, thereby reducing the cross-sectional area of integral panels. To overcome the limitations of these mechanical connections, Liao et al. [1] studied the effect of length, height, and width of a repaired single-edge notched tensile (SENT) structure on gluing repair performance and found that the residual fatigue life can be enhanced by increasing the size of patch. Bouiadjra et al. [7] investigated the effect of shape and thickness of rectangular, trapezoidal, and circular patches on crack initiation, and concluded that the patch shape is sensitive to the panel stacking sequence. Moreover, Lin et al. [8] used the three-dimensional progressive damage analysis method and a cohesive zone model to simulate damage progression and showed that the repair effect heavily depends on the

* Corresponding author at: School of Mechatronics Engineering, Nanchang University, Nanchang 330031, China.
E-mail address: hyfatigue@163.com (Y. Hu).

https://doi.org/10.1016/j.tafmec.2019.102444
Received 25 June 2019; Received in revised form 17 December 2019; Accepted 17 December 2019
Available online 23 December 2019

Nomenclature

Abbreviations

USM	unsharp mask algorithm
HPF	high-pass filter
L-system	Lindenmayer system
LP	laser peening
HEL	Hugoniot elastic limit
FEM	finite element method
XFEM	extended finite element method
MTS	maximum tangential stress criterion

List of symbols

a	crack length
a_0	initial crack length
a_c	critical crack length
A	equivalent integral region
A, B, C, n, M	basic model parameters
c, m	material constants
C_{el}	elastic wave velocity
C_{pl}	plastic wave velocity
$D(i, j)$	strengthened image point
D_i	damage constants, i = 1, 2,3,…., 5
E	elastic modulus
g	template of Gauss filter
$G(x, y)$	gradient amplitude
$G(i, j)$	point filtered by high-pass filter
G_x	gradient operator in horizontal direction
G_y	gradient operator in vertical direction
$I^{(1,2)}$	interaction integral
J	J integral
K_i	stress intensity factor,$i = I, II$
ΔK	amplitude of stress intensity factor
L_p	influence depth of laser peening
N	number of load cycles
$\overline{P}$	average pressure of laser peening
q	boundary function,$0 \leqslant q \leqslant 1$
r, θ	polar coordinates in $x - y$ plane
r_p	radius of plastic zone
$S(i, j)$	original image point
T	T−stress
T^*	normalized temperature
u_i	displacement tensor
$W^{(1,2)}$	interaction strain energy density

Greek letters

σ_e	equivalent stress
σ_{ij}	stress tensor
σ_H	average stress
σ_x, σ_y, τ_{xy}	stress components at crack tip
δ_{1j}	Kronecker symbol
δ_s	yield strength
$\widehat{\theta}$	turning angle
θ_g	gradient direction
$\dot{\varepsilon}_e^*$	normalized equivalent plastic strain rate
ε_e	equivalent plastic strain
ε_f	effective fracture stress
ε_{ij}	strain tensor
τ	pulse width
ρ	material density
λ, μ	Lame material constants
φ	angle between calculating surface and crack surface

thickness of adhesive layer. Furthermore, Usman et al. [9] suggested that temperature can affect crack retardation ability by changing the failure mechanism of materials. In summary, previous research indicates that the gluing repair method is easily affected by process parameters and ambient temperature, which can lead to a lack of shear resistance.

In nature, plant leaf can efficiently withstand long-term alternating loads caused by wind and rain loads. Yohai et al. [10] studied the growing models of plant leaf under the effect of mechanical stress and found that the ability of a leaf to withstand mechanical stress is enhanced by reorientation of the vascular vein in the growing leaf. Pasini [11] noted that the shape and size of petiole cross-sections influence the bending and torsion resistance of leaf. The excellent surface properties and functions of plant leaf are the result of millions of years of optimization and evolution in order to adapt different environments [12]. Veins in plant leaf not only allow water and nutrients to move through the leaf, but also maintain leaf shape and prevent crack propagation [13]. As a result, a bio-inspired concept, in which the non-surface morphology extracted from plant leaf is applied to a metallic surface, has recently been adopted into thermal fatigue, wear, and adhesive failure research [14,15]. In addition, Ritchie et al. [16] observed comparable crack-growth resistance in bio-inspired metal-compliant phase coextruded ceramics. Rajabi [17] reported that insect wings act as barriers to crack propagation. Thus, bionics is a promising method to be adopted to crack research.

Previous crack growth research has also shown that residual stress plays a key role in crack propagation [18,19]. The cross-scale crack evolution problem exists in both aircraft skin and plant leaf under the effect of alternating loads, whereby the material is more likely to experience mechanical fatigue cracking instead of thermal fatigue, wear, or adhesive failure. Therefore, based on the veins of a plant leaf, this study proposes a bio-inspired method to improve the crack resistance of aluminum alloys which are widely used in aircraft skins. According to biological couplings' properties, biological couplings can be classified into geometric, mathematic, physical, chemical, integrated, and mechanical biological couplings [20]. This study adopts mechanical biological coupling, in which coupling elements are formed by methods such as embedment, combination, and coalescence. To achieve mechanical biological coupling in this study, a biomimetic stress field inspired by plant leaf veins is obtained via laser peening and applied to aluminum alloy surface. The main goal of this research is to explore the effectiveness of introducing this biomimetic stress field on the crack resistance of aluminum alloy.

2. Constructing the bio-inspired structure simulation model

2.1. Plant leaf feature extraction

Inspired by the observation that plant leaf can bear long-term alternating loads without cracking, the plant leaf vein structure is extracted to analyze the mechanism of crack retardation. As plant veins exhibit a crisscross structure and have the characteristics of self-similarity and scale invariance, the method proposed by Mandelbrot [21] is adopted to extract the vein structure of plant leaf, in which irregular structures with self-similar hierarchical morphology can be effectively rebuilt. In order to improve the extraction accuracy, a dicotyledon rosaceae plum leaf is adopted due to its relatively developed venation structure. The fractal angle (the angle between primary and secondary veins), branch growth ratio (the length ratio between secondary and primary veins), and initial growth point (the initial fractal point set) are

extracted firstly. Then, the method proposed by Mandelbrot [21] is used to reconstruct the plant leaf vein structure. For the edges of vein features are blurred, the vein information located in high frequency part of image can be visualized by using a grayscale histogram, as shown in Fig. 1.

In addition, the unsharp mask (USM) sharpening algorithm [22] is used to strengthen the high-frequency details of the vein edge for an original image point $S(i,j)$. The principle diagram of the USM algorithm is shown in Fig. 2. $G(i,j)$ is the point filtered by high-pass filter (HPF) and $D(i,j)$ is the strengthened image point.

The template for Gauss filter, g, used in HPF is given in Eq. (1).

$$g = \begin{bmatrix} -1 & -1 & -1 \\ -1 & 8 & -1 \\ -1 & -1 & -1 \end{bmatrix} \tag{1}$$

The image strengthened by USM is shown in Fig. 3.

The Canny edge detection operator [23], which is commonly used in image edge detection, is adopted in this study. The basic concept of this algorithm is to search the area with the most dramatic image gradient changes. This area is measured by gradient amplitude $G(x,y)$ and gradient direction θ_g, shown in Eq. (2).

$$\begin{cases} G(x,y) = \sqrt{G_x^2 + G_y^2} \\ \theta_g = tan^{-1}(G_x/G_y) \end{cases} \tag{2}$$

where G_x and G_y are gradient operators in horizontal and vertical directions, respectively. More details on Canny edge detection could be found in Ref. [23].

Finally, the features of main and secondary veins are extracted by Hough transform [24] after Canny edge detection, in which the extracted vein feature points are mapped to the parameter space then converted into line and angle information, as shown in Fig. 4. More details on the Hough transform could be found in Ref. [24]

The absolute difference in the angle between primary and secondary veins is calculated according to the slope information of the obtained straight line. The statistical angle difference ranges from 41.1° to 60.1°. Considering the demands of model design, the value space of fractal angle is defined as [40°, 60°] and interval value is 5°. The detected length ratio between secondary vein and main vein is approximately 2/3, which is defined as branch growth ratio.

It is generally believed that the crack tip experiences maximum stress concentration and that the crack path is a collection of stress concentration points of each periodic extension process. Because fatigue cracks have self-similar fractal properties and can be considered as a fractal set [25], the potential stress concentration area is suggested to be covered by bio-inspired structure. The Cantor middle-third set [26], a method for constructing a collection of self-similar fractal sets, is adopted to establish the initial crack fractal point set. The initial fractal point set is then used as initial growth point of the bio-inspired structure. A flow chart of the algorithm for Cantor middle - third set is shown in Fig. 5.

2.2. Finite element simulation model construction

The rewriting rule of Lindenmayer System (L-system) for plant leaf veins [27], which is established using the Mandelbrot fractal method, is used to rebuild the plant leaf veins, as shown in Eq. (3):

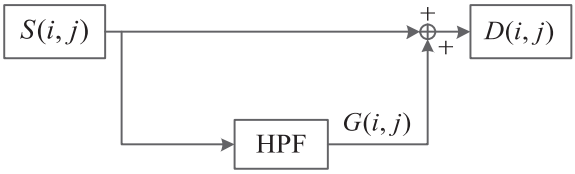

Fig. 2. Principle diagram of USM algorithm.

$$\begin{aligned} &v: \{A, B, [], ()\} \\ &w: A \\ &P: A \rightarrow AA, B \rightarrow A[B]B(B) \end{aligned} \tag{3}$$

where A represents a drawing of the main vein, B represents a drawing of the secondary vein, "[]" denotes the left-turn degree of the control branch, and "()" represents the right-turn angle of the control branch.

The bio-inspired surface is then constructed using the above feature extractions. The initial crack Cantor middle-third set obtained according to Fig. 5 is considered as growth point, the angle between primary and secondary veins is selected as fractal angle, and the length ratio between secondary and primary veins is selected as branch growth ratio. Combined with the L-system growth rule, five different types of bio-inspired residual stress fields are generated on the surface of specimens by using laser peening (LP). The magnitude of the applied residual stress is determined according to Ref. [28], in which the residual stress field was also obtained by laser peening. In addition, the stress distribution in depth direction is determined by Eq. (4) [29]:

$$\begin{cases} L_p = \left(\frac{C_{el}C_{pl}\tau}{C_{el} - C_{pl}}\right)\left(\frac{\overline{P} - HEL}{2HEL}\right) \\ C_{el} = \sqrt{\frac{\lambda + 2\mu}{\rho}} \\ C_{pl} = \sqrt{\frac{\lambda + 2\mu/3}{\rho}} \end{cases} \tag{4}$$

where L_p is the influence depth of laser peening, C_{el} is the elastic wave velocity, C_{pl} is the plastic wave velocity, and $\overline{P}$ is the average pressure of laser peening. Hugoniot elastic limit (HEL) is the highest elastic limit of the material, τ is the pulse width, $\rho$is the material density, $\lambda$and$\mu$are the Lame constants of the material.

The bio-inspired surface area and residual stress distribution of the bio-inspired structure for compact tension specimen are shown in Fig. 6.

3. Stress intensity factor calculation

In order to improve the accuracy of the analysis results, a C3D8R linear reduction integral element [30], which is a continuum three-dimensional brick element with eight nodes, is used to complete the mesh division for the specimen. An R3D4 bilinear element [30], which is a rigid three-dimensional element with four nodes, is used to construct a discrete rigid body to simulate the tension fixture. The crack tip expansion function constructed by the extended finite element method (XFEM) level set is used to simulate the crack contact information.

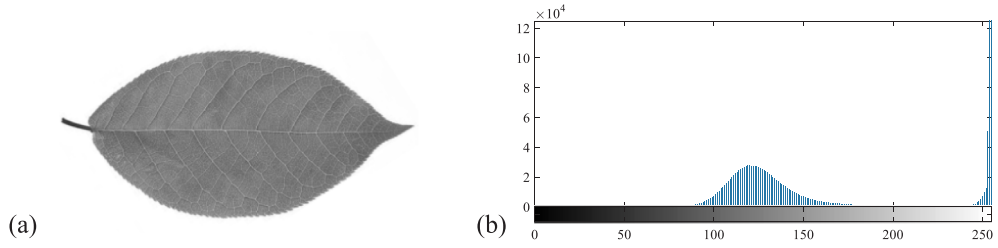

Fig. 1. Grayscale transform for plant leaf: (a) grayscale image of leaf and (b) grayscale histogram.

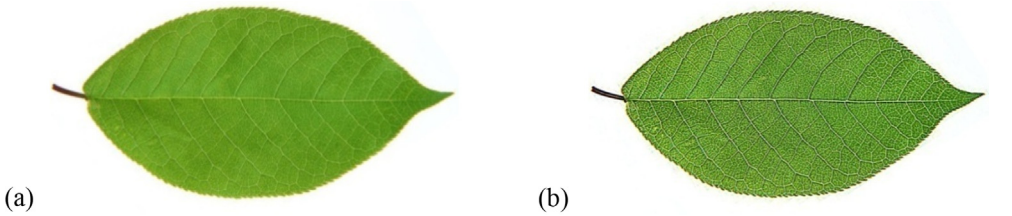

Fig. 3. Vein image strengthened by USM: (a) original image and (b) USM strengthened image.

Laser peening is a surface strengthened method accompanied by a high material strain rate, and the Johnson-Cook constitutive relationship is an effective solution for the dynamic response caused by LP impact loads [31]. Thus, the Johnson-Cook constitutive equation is adopted to establish the damage failure model. The yield stress form for joints is as follows:

$$\sigma_e = (A + B\varepsilon_e^n)\cdot(1 + C\ln\dot{\varepsilon}_e^*)\cdot\left(1 - T^{*m}\right) \tag{5}$$

where σ_e is the equivalent stress, ε_e is the equivalent plastic strain, $\dot{\varepsilon}_e^*$ is the normalized equivalent plastic strain rate, T^* is the normalized temperature, and A, B, C, n, and M are the basic model parameters determined by Ref. [32] and shown in Table. 1.

The fracture stress form for joints is as follows:

$$\varepsilon_f = \left(D_1 + D_2\exp\left(D_3\frac{\sigma_H}{\sigma_e}\right)\right)\cdot(1 + D_4\ln\dot{\varepsilon}_e^*)\cdot(1 - D_5T^*) \tag{6}$$

where ε_f is the fracture stress, σ_e is the average stress, and D_i (i = 1, 2,3, …, 5) are damage constants determined by Ref. [33] and shown in Table. 2.

The interaction integral method [34] is adopted to calculate the stress intensity factors at the crack tip of the bio-inspired structure. It is assumed that the finite element method (FEM) solutions at the crack tip of the bio-inspired structure are $\sigma_{ij}^{(1)}$, $\varepsilon_{ij}^{(1)}$, $u_i^{(1)}$, and $K_{\mathrm{I}}^{(1)}$, and the respective analytical solutions are $\sigma_{ij}^{(2)}$, $\varepsilon_{ij}^{(2)}$, $u_i^{(2)}$ and $K_{\mathrm{I}}^{(2)}$. Subscripts i, j are coded as 1, 2 to represent the x and y coordinates of the crack tip. According to the principle of superposition for elasticity, these solutions can be written as the following superposed solutions:

$$\begin{cases} \sigma_{ij} = \sigma_{ij}^{(1)} + \sigma_{ij}^{(2)} \\ \varepsilon_{ij} = \varepsilon_{ij}^{(1)} + \varepsilon_{ij}^{(2)} \\ u_i = u_i^{(1)} + u_i^{(2)} \\ K_{\mathrm{I}} = K_{\mathrm{I}}^{(1)} + K_{\mathrm{I}}^{(2)} \end{cases} \tag{7}$$

Then, the J integral can be written as follows:

$$J = \int_A \left(\sigma_{ij}\frac{\partial u_i}{\partial x_1} - \frac{\sigma_{ij}\varepsilon_{ij}}{2}\delta_{1j}\right)\frac{\partial q}{\partial x_j}dA \tag{8}$$

where δ_{1j} is the Kronecker symbol given by Eq. (9).

$$\delta_{1j} = \begin{cases} 1 & j = 1 \\ 0 & j = 2 \end{cases} \tag{9}$$

Here, A is the equivalent integral region and q is the boundary function of region A, shown in Fig. 7.

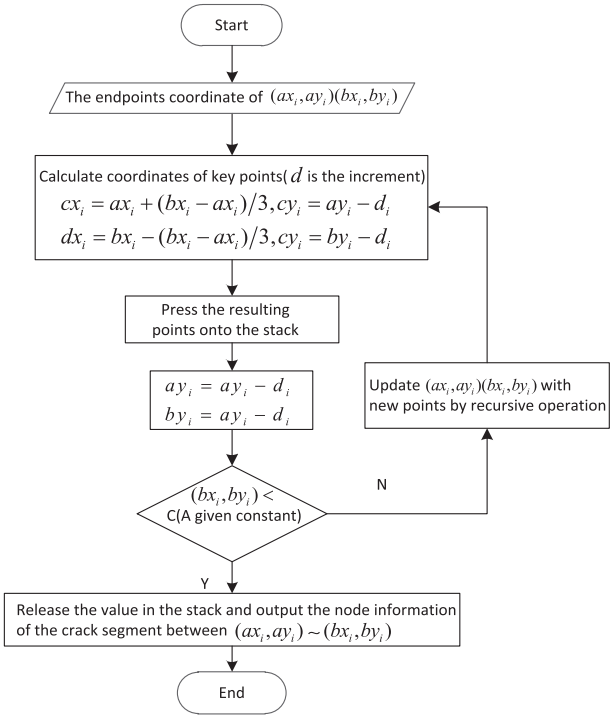

Fig. 5. Algorithm for calculating the initial growth point of the bio-inspired structure.

The interaction integral $I^{(1,2)}$ can be written as follows:

$$I^{(1,2)} = \int_A \left(\frac{\sigma_{ij}^{(1)}\partial u_i^{(2)} + \sigma_{ij}^{(2)}\partial u_i^{(1)}}{\partial x_1} - W^{(1,2)}\delta_{1j}\right)\frac{\partial q}{\partial x_j}dA \tag{10}$$

where $W^{(1,2)}$ is the strain energy density, defined as follows:

$$W^{(1,2)} = \sigma_{ij}^{(1)}\varepsilon_{ij}^{(2)} = \sigma_{ij}^{(2)}\varepsilon_{ij}^{(1)} \tag{11}$$

By substituting Eq. (7) into Eq. (8), the J integral of the superposition state can be written as follows:

$$J = J^{(1)} + J^{(2)} + I^{(1,2)} \tag{12}$$

The relationship between J integral and stress intensity factor of the

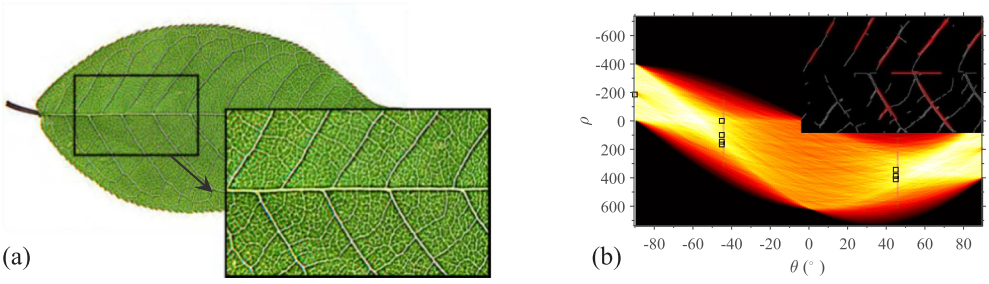

Fig. 4. Results of plant leaf feature extraction: (a) vein angle feature extraction and (b) Hough transform detection results.

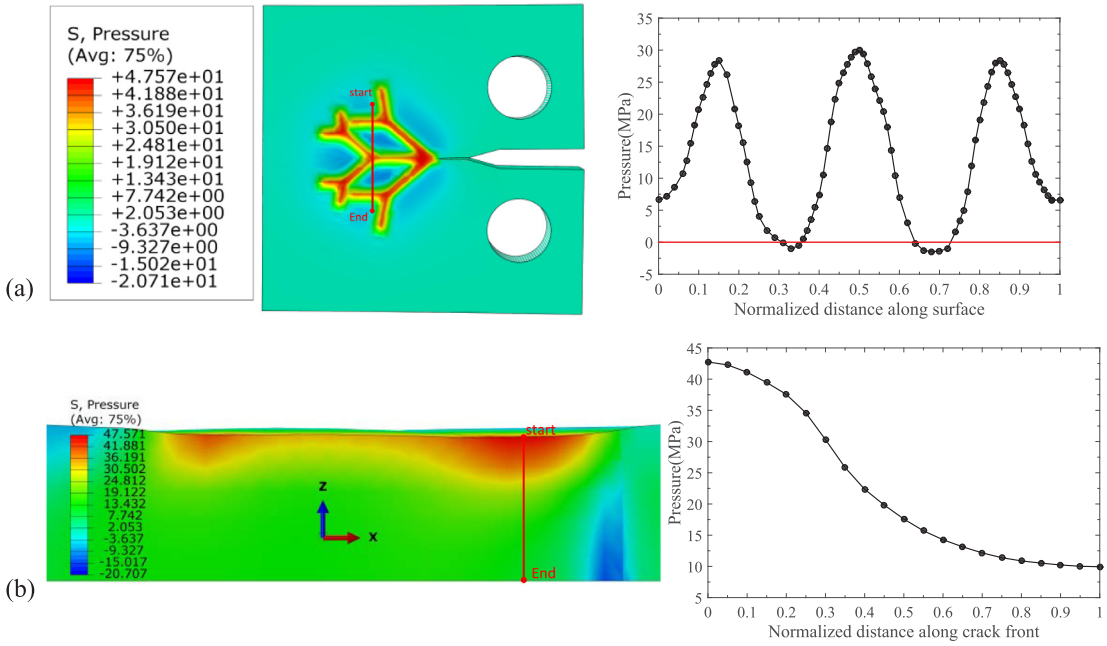

Fig. 6. Pressure distribution of the bio-inspired residual stress field (red line represents the path). (a) on the surface, and (b)along with depth. (For interpretation of the references to colour in this figure legend, the reader is referred to the web version of this article.)

Table 1
Yield parameters of the Johnson-cook constitutive equation.

A (MPa)	B (MPa)	n	M	C	Melting temp (K)	Transition temp (K)
352	440	0.42	1.7	0.0083	775	293

Table 2
Damage parameters of the Johnson-cook constitutive equation.

D_1	D_2	D_3	D_4	D_5	Melting temp (K)	Transition temp (K)
0.13	0.13	−1.5	0.011	0	775	293

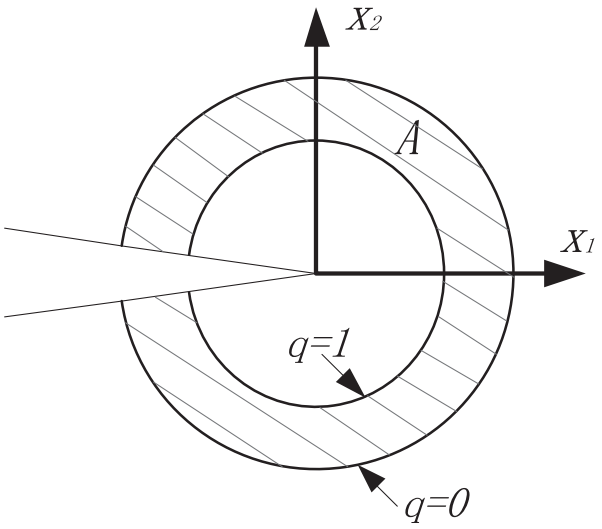

Fig. 7. Interaction integral path.

superposition state is written as:

$$J = J^{(1)} + J^{(2)} + \frac{2}{E}K_I^{(1)}K_I^{(2)} \tag{13}$$

where E is the elastic module.

Combined with Eq. (12) and Eq. (13), the relationship between interaction integral and stress intensity factors is obtained as follows:

$$I^{(1,2)} = \frac{2}{E}K_I^{(1)}K_I^{(2)} \tag{14}$$

It should be noted that $K_{\mathrm{I}}^{(1)} = K_{\mathrm{I}}$ and $K_{\mathrm{I}}^{(2)} = 1$ when mode I crack [1] is investigated; thus, the stress intensity factor is obtained as follows:

$$K_{\mathrm{I}} = K_{\mathrm{I}}^{(1)} = \frac{E}{2}I^{(1,2)} \tag{15}$$

4. Stress intensity factor calculation results and discussions

The boundary conditions of the bio-inspired structure are illustrated in Fig. 8. The material of the specimen is 2024-aluminum alloy, which is widely used for aircraft skin. The amplitude of the uniaxial tension load is 2.2 kN, the stress ratio is 0.1, and the frequency is 10 Hz.

4.1. Effects of the bio-inspired structure on crack turning

Predicting crack turning is a complex problem that involves the calculation of stress components and displacement components. Many criteria have been proposed to investigate this problem. In this study,

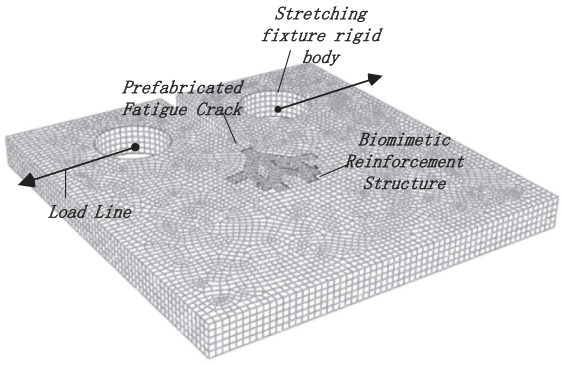

Fig. 8. Finite element model of the bio-inspired structure.

the maximum tangential stress criterion (MTS) is adopted [35]. The turning angle $\hat{\theta}$ is calculated as follows:

$$\hat{\theta} = \cos^{-1}\left(\frac{3K_{II}^2 + \sqrt{K_I^4 + 8K_I^2K_{II}^2}}{K_I^2 + 9K_{II}^2}\right) \tag{16}$$

Fig. 9 shows the crack propagation path simulation results, which indicate that the crack propagation path of the bio-inspired structure is deflected, unlike the crack propagation path of the original specimen. Moreover, the crack is deflected from one direction to another in plant leaf due to being blocked by the veins, subsequently propagating in the direction of another vein (Fig. 9(c)). This reveals that the bio-inspired structure improves crack resistance by increasing the crack length and energy consumption.

4.2. Effects of fractal angle on the stress intensity factor

The calculation results of the stress intensity factor (K_I) at different fractal angles are shown in Fig. 10(a) and the decrease in K_I at different fractal angles are shown in Fig. 10(b). The stress intensity factor of the specimens with a bio-inspired structure are significantly lower than that of the untreated specimen (Fig. 10(b)). Crack retardation in bio-inspired structure first increases then decreases as crack length increases. Notably, the maximum reduction of K_1 is 31.24% for a crack length of 6 mm while fractal angle is of 60°.

4.3. Effects of depth on the stress intensity factor

In order to evaluate the effects of depth on the stress intensity factor, the value of K_I along the crack front is shown in Fig. 11. The bio-inspired structure is mapped on the surface with a normalized distance of "0". The value of K_I first increases then decreases slightly along the crack front. Combined with Fig. 6(b), the pressure changes dramatically within a normalized distance of approximately 0.5, which corresponds to the trend of $K_\mathrm{I}$along the crack front. Thus, the effects of the bio-inspired structure on the stress intensity factor are closely related to the depth as well as the pressure distribution.

4.4. Effects of thickness on the stress intensity factor

Kotousov reported that the stress state intensity is significantly influenced by the material thickness [36,37]. To investigate the effects of thickness on the stress intensity factor, specimens with a thickness of 5 mm, 8 mm, and 11 mm are analyzed. The comparison results are shown in Fig. 12. With increasing thickness, the stress intensity factor decreases, which indicates that increasing the specimen thickness can also retard crack growth. However, if lightweight is the primary consideration during the design process, the bio-inspired structure method is a preferable choice.

4.5. Comparison of the crack resistance performance for different methods

In order to investigate the effect of the proposed method on crack resistance, specimens strengthened by square-shaped laser peening, full-coverage laser peening, square criss-cross pattern peening and the SENT repair method [1] are compared. The boundary conditions for these models are given in Fig. 13 and the stress intensity factor calculation results are plotted in Fig. 14. It's clear that the stress intensity factor results are similar for the square-shaped and full-coverage laser peening methods. In comparison, the stress intensity factors of the proposed method, the SENT specimen repair method, and the square criss-cross pattern method are substantially smaller. The square-shaped and full-coverage laser peening methods exhibit weak crack resistance because the specimen tends to be unstable under the action of high-stress density, which was validated by Dorman [38]. Moreover, the SENT specimen repair method requires a patch to be glued onto the specimen to retard crack growth, which results in weight increase. In contrast, the proposed method achieves the lowest stress intensity factors without the need to add patches to the specimen. Compared with the proposed model, the square criss-cross pattern is weak in improving crack resistance while the crack length is less than 6 mm, and the stress intensity factor calculation results are slightly higher than the proposed model when the crack length is longer than 6 mm.

4.6. Effects of plastic zone on the stress field around the crack tip

The stress field at the crack tip can be simplified as a plane stress problem, as shown in Fig. 15, where r and θ are the polar coordinates in the x-y plane and σ_x, σ_y, and τ_{xy} are the stress components on a micro-body around the crack tip.

The von Mises yield criterion [39] is adopted to determine the plastic zone. As the elastic T term is a nonsingular term during the crack growth process, it is suggested that the T term has an important effect on the stress field around the crack tip. In order to investigate the effects of the bio-inspired structure on plastic zone more accurately, the modified plastic zone under the effect of T stress is obtained by using the Dugdale model [40]:

$$r_p = \pi\sin^2\varphi(1 + \cos\varphi)K_I^2/[64(\delta_s + T\sin\varphi\cos\varphi)^2] \tag{17}$$

where r_p is the calculated radius of the plastic zone, φ is the angle between the calculation surface and the crack surface, and δ_s is the yield strength.

The shape of plastic zone at the crack tip for different bionic parameters is shown in Fig. 16, which shows that the plastic zone is enlarged compared with the untreated structure. In addition, the decreasing trend of the stress intensity factor shown in Fig. 10(a) corresponds to the expanding trend of the plastic zone. In order to better understand the stress decrease mechanism caused by plastic deformation, the stress distributions around the crack tip are shown in Fig. 17. According to Fig. 17, the effects of the bio-inspired structure on the stress field are dominant in the plastic zone. With increasing distance from the crack tip, the effects of fractal parameters on the stress field are reduced, resulting in a gradual decrease of crack resistance strengthening by the bio-inspired structure. This shows that the effects of bio-inspired structure on crack resistance are closely related to the size and shape of the plastic zone, which is consistent with the stress

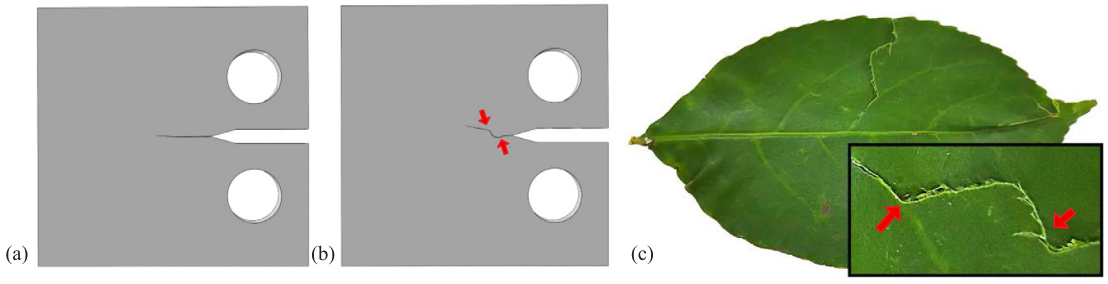

Fig. 9. Crack propagation path: (a) untreated sample, (b) biomimetic enhanced sample, and (c) crack path along the leaf.

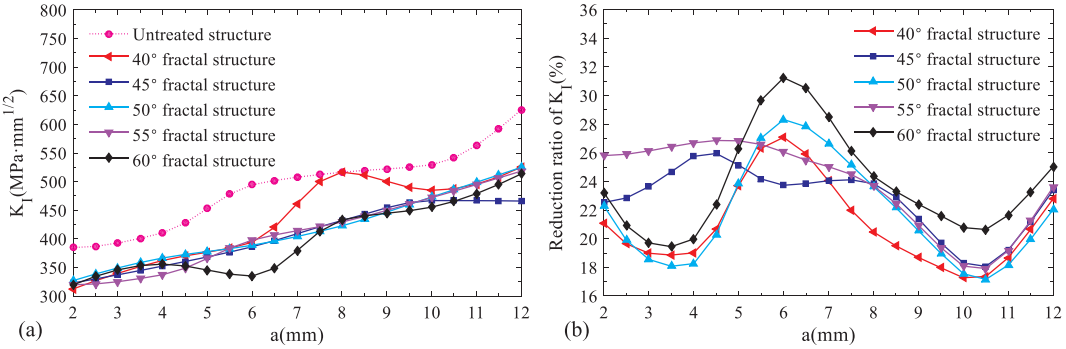

Fig. 10. Distributions of K_I with different fractal structures: (a) trend of K_I with fractal angle and (b) reduction ratio of K_I with different fractal angles.

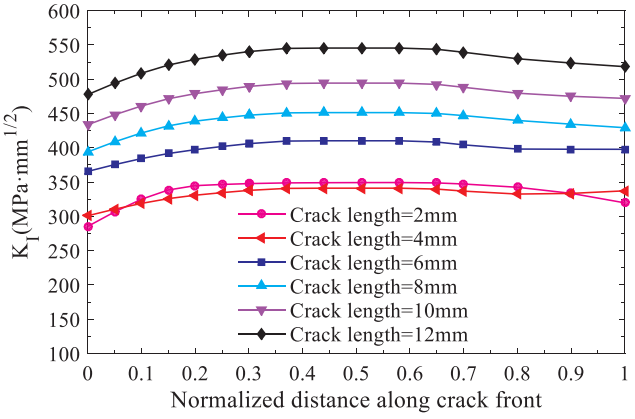

Fig. 11. Distribution of K_I along depth.

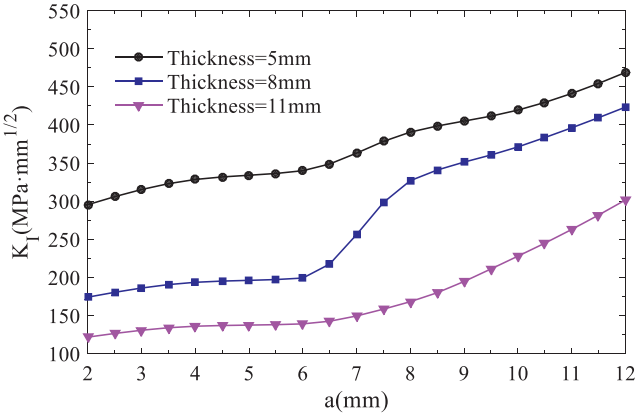

Fig. 12. a–K_I curves corresponding to different specimen thicknesses.

shielding theory proposed by Irwin [41].

5. Residual fatigue life prediction and analysis

5.1. Residual fatigue life prediction model

The prediction of residual fatigue life has key engineering significance in the design of aircraft skin with damage tolerance. It is common to use Paris formula to predict the residual fatigue life [42]:

$$\frac{da}{dN} = c(\Delta K)^m \tag{18}$$

where N is the number of load cycles, c and m are material constants obtained from fatigue tests, and ΔK is the amplitude of the stress intensity factor.

The residual fatigue life is obtained by integrating Eq. (18) as follows:

$$N = \int_{a_0}^{a_c} \frac{1}{c(\Delta K)^m} da \tag{19}$$

where a_0 is the initial crack length and a_c is the critical crack length.

5.2. Residual fatigue life of different bio-inspired structures

The residual fatigue life calculation results according to different bio-inspired structures are plotted in Fig. 18. The results for specimens strengthened by bio-inspired structures are substantially improved compared with those of untreated specimens. The residual fatigue life values for fractal angles of 40°, 45°, 50°, 55°, and 60° are 8.4×10^4, 9.5×10^4, 8.6×10^4, 1.0×10^5, and 9.5×10^4, which are 154.5%, 187.8%, 160.6%, 203.0%, and 187.8% higher than those of the untreated specimens (3.3×10^4), respectively. The specimen with a fractal angle of 55° exhibited the best crack resistance effect.

5.3. Residual fatigue life with different strengthening methods

In order to evaluate the crack resistance performance of the proposed method, a square-shaped laser peening specimen, a full-coverage laser peening specimen, a square criss-cross pattern peening specimen and a SENT repair specimen [1] are compared. Fig. 19 clearly shows that the proposed method, the square criss-cross pattern method and the SENT specimen repair method [1] exhibit substantially crack resistance than the other two methods. Specifically, the proposed method achieves the best crack resistance performance, with a residual fatigue life nearly 1.23 times of the square criss-cross pattern method, two times that of the SENT specimen repair method, three times that of the square-shaped laser peening method. In addition, as lightweight is a key consideration in aircraft design, the SENT specimen repair method would be less attractive because of the weight increase caused by the glued patch. Thus, the proposed method is clearly superior in terms of crack resistance improvement.

5.4. Residual fatigue life for different initial crack lengths

This section briefly discusses the effects of initial crack length on crack growth. As shown in Fig. 20, specimens with initial crack lengths of 1 mm, 2 mm, and 3 mm are adopted. All the three specimens are analyzed till crack extends to 8 mm. As the initial crack length increases, the residual crack fatigue life decreases, which indicates that the initial crack length has an important effect on the crack resistance of the proposed method.

6. Conclusions

Inspired by the crack resistance exhibited by plant leaf, a bio-inspired method is proposed to improve the crack resistance of aluminum alloy material used for aircraft skin, in which a biomimetic residual

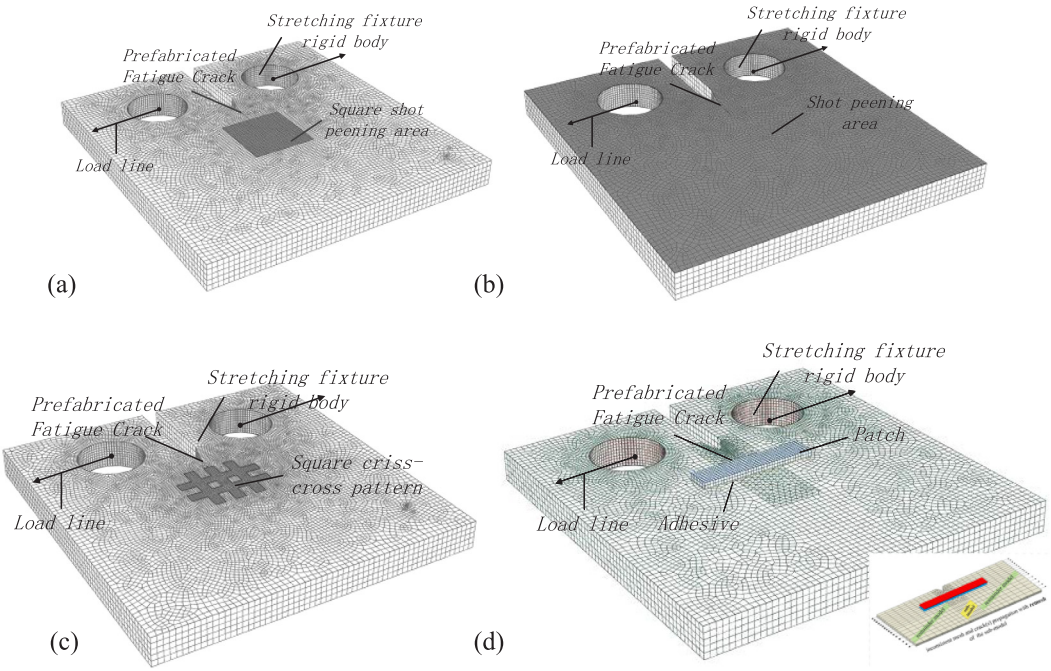

Fig. 13. Boundary conditions for different simulation models: (a) square-shaped laser peening, (b) full-coverage laser peening, (c) square criss-cross peening, and (d) the SENT specimen repair method [1].

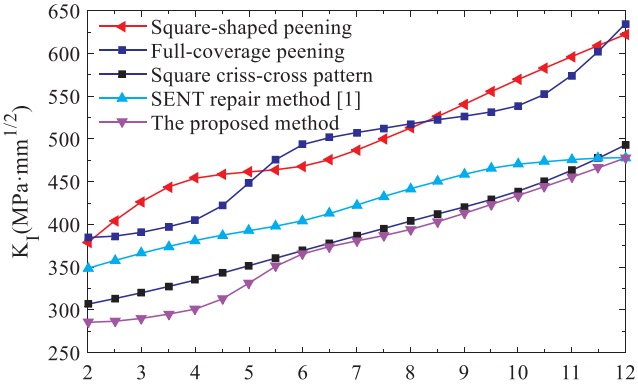

Fig. 14. Stress intensity factor curves for different strengthening methods.

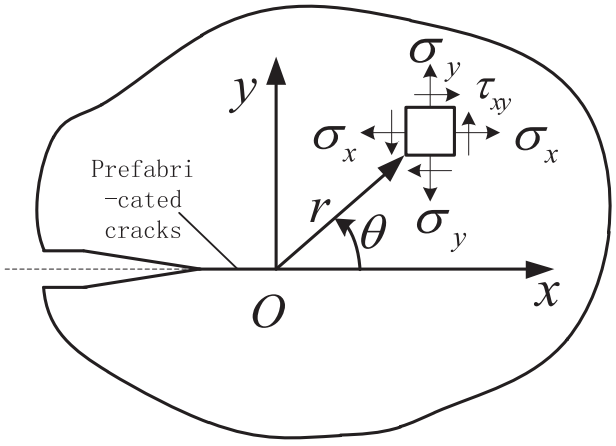

Fig. 15. Generalized plane stress element.

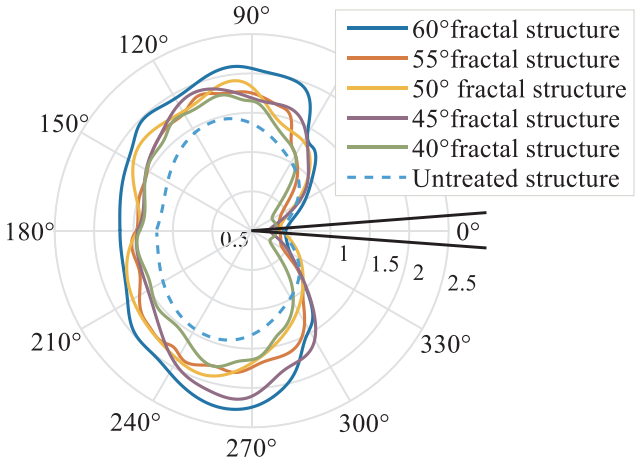

Fig. 16. Morphological changes in the plastic zone for different fractal angles.

stress field is applied to the crack tip. The following conclusions are obtained:

(1) Crack turning is observed during crack growth in the bio-inspired structure, which reveals that the crack resistance is improved due to an increase in crack length and energy consumption. A maximum reduction in the stress intensity factor of 31.24% is observed for a crack extension of 6 mm and a fractal angle of 60°. This indicates that the bio-inspired method can effectively relieve stress concentration around the crack tip.

(2) The thickness of the specimen has a positive effect on crack resistance; however, this effect is limited by the design requirements for a lightweight. Compared with the square-shaped laser peening method, full-coverage laser peening method, the square criss-cross pattern method and SENT specimen repair method, the proposed method achieves the best crack resistance performance.

(3) The plastic zone is enlarged compared with the untreated structure; the reduction in the stress intensity factor corresponds to this enlargement of the plastic zone. In addition, the effects of the bio-

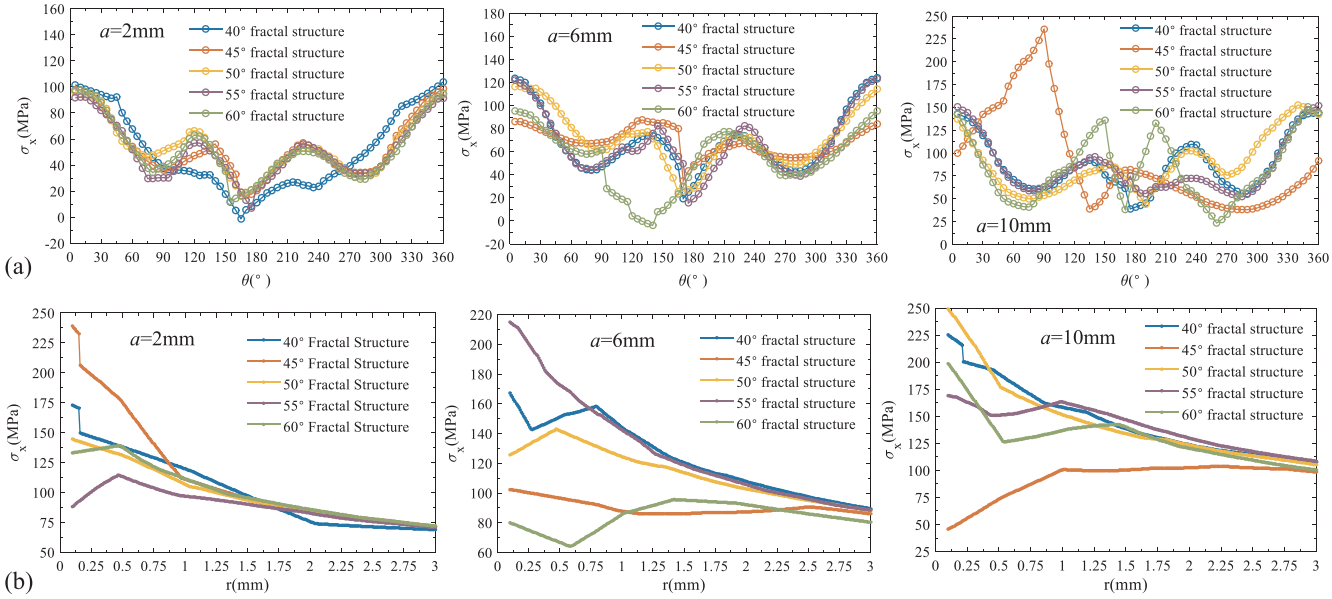

Fig. 17. Stress distribution around the crack tip for different fractal structures: (a) circumferential stress distribution and (b) radial stress distribution.

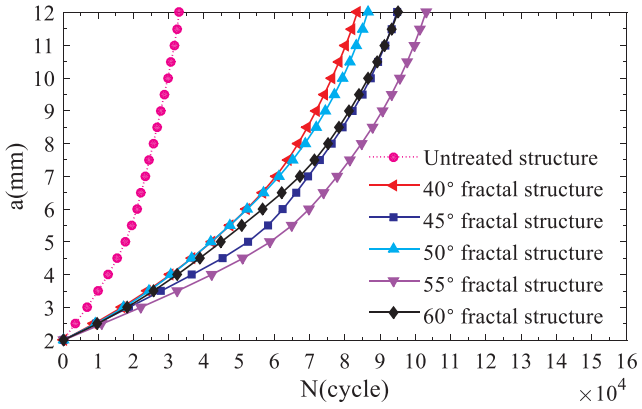

Fig. 18. Fatigue life of specimens with different fractal angles.

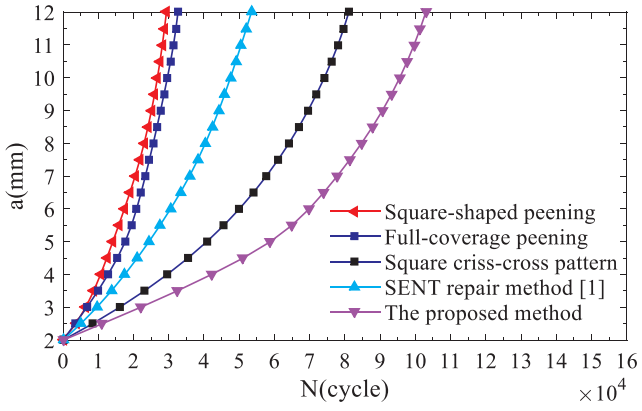

Fig. 19. Fatigue life of specimens with different strengthening methods.

inspired structure are closely related to the size and shape of the plastic zone, which is consistent with the stress shielding theory.

(4) Compared with the untreated specimens, the residual fatigue life of specimens strengthened by the proposed approach is increased by up to 203.0%. Moreover, compared with the other strengthening methods, the residual fatigue life is the longest for specimens strengthened by the proposed method, and nearly three times that of specimens strengthened by the square- pattern laser peening method, which exhibits the lowest residual fatigue life. Thus, the proposed method is predicted to retard crack growth in aluminum alloy aircraft skin material.

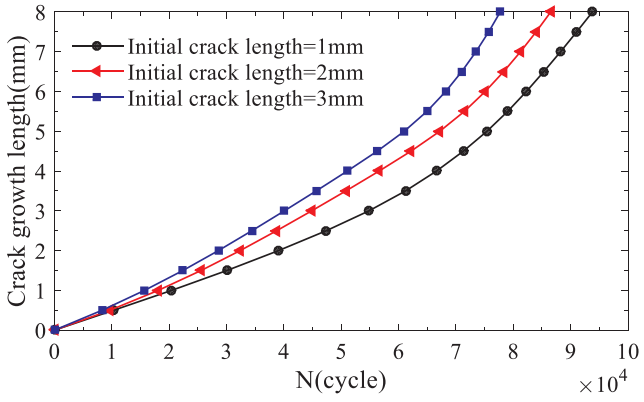

Fig. 20. Residual fatigue life of specimens with different initial crack lengths.

Declaration of Competing Interest

The author declare that there is no conflict of interest.

Acknowledgments

The authors would like to gratefully acknowledge the support of the project of the National Natural Science Foundation of China, China [Grant number. 51705229], and the support of China Scholarship Council, China.

Appendix A. Supplementary material

Supplementary data to this article can be found online at https://doi.org/10.1016/j.tafmec.2019.102444.

References

[1] Y. Liao, Y. Li, Q. Pan, M. Huang, C. Zhou, Residual fatigue life analysis and comparison of an aluminum lithium alloy structural repair for aviation applications,

Eng. Fract. Mech. 194 (2018) 262–280, https://doi.org/10.1016/j.engfracmech.2018.03.020.
[2] Y. Zhang, B. Chen, A. Liu, Y. lin Pi, J. Zhang, Y. Wang, L. Zhong, Experimental study on shear behavior of high strength bolt connection in prefabricated steel-concrete composite beam, Compos. Part B Eng. 159 (2019) 481–489. https://doi.org/10.1016/j.compositesb.2018.10.007.
[3] H. Guo, F. Xiao, Y. Liu, G. Liang, Experimental and numerical study on the mechanical behavior of Q460D high-strength steel bolted connections, J. Constr. Steel Res. 151 (2018) 108–121, https://doi.org/10.1016/j.jcsr.2018.09.012.
[4] W.Z. Zhuang, Prediction of crack growth from bolt holes in a disc, Int. J. Fatigue. 22 (2000) 241–250, https://doi.org/10.1016/S0142-1123(99)00122-X.
[5] V.K. Babbar, P.R. Underhill, C. Stott, T.W. Krause, Finite element modeling of second layer crack detection in aircraft bolt holes with ferrous fasteners present, NDT E Int. 65 (2014) 64–71, https://doi.org/10.1016/j.ndteint.2014.03.005.
[6] A.A. Abd-Elhady, H.E.D.M. Sallam, Crack sensitivity of bolted metallic and polymeric joints, Eng. Fract. Mech. 147 (2015) 55–71, https://doi.org/10.1016/j.engfracmech.2015.08.005.
[7] M.A. Caminero, S. Pavlopoulou, M. Lopez-Pedrosa, B.G. Nicolaisson, C. Pinna, C. Soutis, Analysis of adhesively bonded repairs in composites: damage detection and prognosis, Compos. Struct. 95 (2013) 500–517, https://doi.org/10.1016/j.compstruct.2012.07.028.
[8] G. Lin, P. Chen, PDA-CZM method for failure analysis of bonded repair of composite laminates, Acta Aeronaut Astronaut Sin, 30 (2009) 1877–1882. https://www.researchgate.net/publication/293151476.
[9] M. Usman, J.A. Pascoe, R.C. Alderliesten, R. Benedictus, The effect of temperature on fatigue crack growth in FM94 epoxy adhesive bonds investigated by means of energy dissipation, Eng. Fract. Mech. 189 (2018) 98–109, https://doi.org/10.1016/j.engfracmech.2017.10.007.
[10] Y. Bar-Sinai, J.D. Julien, E. Sharon, S. Armon, N. Nakayama, M. Adda-Bedia, A. Boudaoud, Mechanical stress induces remodeling of vascular networks in growing leaves, PLoS Comput. Biol. 12 (2016) 1–21, https://doi.org/10.1371/journal.pcbi.1004819.
[11] D. Pasini, On the biological shape of the Polygonaceae Rheum Petiole, Int. J. Des. Nat. 4 (2009) 97–104, https://doi.org/10.2495/D&NE-V3-N1-39-64.
[12] C. an Wang, Y. Huang, Q. Zan, H. Guo, S. Cai, Biomimetic structure design – a possible approach to change the brittleness of ceramics in nature, Mater. Sci. Eng. C. 11 (2000) 9–12. https://doi.org/10.1016/S0928-4931(00)00133-8.
[13] Z. Zhang, L. Ren, H. Zhou, Z. Han, X. Tong, Y. Zhao, L. Chen, Effect of thermal fatigue loading on tensile behavior of H13 die steel with biomimetic surface, J. Bionic Eng. 7 (2010) 390–396, https://doi.org/10.1016/S1672-6529(10)60271-5.
[14] C. Meng, H. Zhou, H. Zhang, X. Tong, D. Cong, C. Wang, L. Ren, The comparative study of thermal fatigue behavior of H13 die steel with biomimetic non-smooth surface processed by laser surface melting and laser cladding, Mater. Des. 51 (2013) 886–893, https://doi.org/10.1016/j.matdes.2013.05.005.
[15] J. Liu, Z. Zhang, Z. Yu, Y. Liang, X. Li, L. Ren, Experimental study and numerical simulation on the structural and mechanical properties of Typha leaves through multimodal microscopy approaches, Micron. 104 (2018) 37–44, https://doi.org/10.1016/j.micron.2017.10.004.
[16] R.P. Wilkerson, B. Gludovatz, J. Watts, A.P. Tomsia, G.E. Hilmas, R.O. Ritchie, A study of size effects in bioinspired, “nacre-like”, metal-compliant-phase (nickel-alumina) coextruded ceramics, Acta Mater. 148 (2018) 147–155, https://doi.org/10.1016/j.actamat.2018.01.046.
[17] H. Rajabi, A. Darvizeh, A. Shafiei, D. Taylor, J.H. Dirks, Numerical investigation of insect wing fracture behaviour, J. Biomech. 48 (2015) 89–94, https://doi.org/10.1016/j.jbiomech.2014.10.037.
[18] D. Tchuindjang, W. Fricke, M. Vormwald, Numerical analysis of residual stresses and crack closure during cyclic loading of a longitudinal gusset, Eng. Fract. Mech. 198 (2018) 65–78, https://doi.org/10.1016/j.engfracmech.2017.08.018.
[19] A. Jacob, A. Mehmanparast, R. D’Urzo, J. Kelleher, Experimental and numerical investigation of residual stress effects on fatigue crack growth behaviour of S355 steel weldments, Int. J. Fatigue. 128 (2019) 105196, https://doi.org/10.1016/j.ijfatigue.2019.105196.
[20] L. Ren, Y. Liang, Biological couplings: classification and characteristic rules, Sci. China Ser. E Technol. Sci. 52 (2009) 2791–2800, https://doi.org/10.1007/s11431-009-0325-8.
[21] B.B. Mandelbrot, J.A. Wheeler, The fractal geometry of nature, Am. J. Phys. 51 (1983) 286–287, https://doi.org/10.1119/1.13295.
[22] J.A. Ferrari, J.L. Flores, C.D. Perciante, E. Frins, Edge enhancement and image equalization by unsharp masking using self-adaptive photochromic filters, Appl. Opt. 48 (2009) 3570–3579, https://doi.org/10.1364/AO.48.003570.
[23] L. Ding, A. Goshtasby, On the Canny edge detector, Pattern Recognit. 34 (2001) 721–725. https://doi.org/https://doi.org/10.1016/S0031-3203(00)00023-6.
[24] M. FOKKINGA, The Hough transform, J. Funct. Program. 21 (2011) 129–133. https://doi.org/DOI: 10.1017/S0956796810000341.
[25] L. Molent, A. Spagnoli, A. Carpinteri, R. Jones, Using the lead crack concept and fractal geometry for fatigue lifing of metallic structural components, Int. J. Fatigue. 102 (2017) 214–220, https://doi.org/10.1016/j.ijfatigue.2017.04.001.
[26] K. Williamson, A. Saigal, Modeling self-similar dendrite arrays with a cantor middle-third set of line segments, Comput. Mater. Sci. 6 (1996) 343–349. https://doi.org/https://doi.org/10.1016/0927-0256(96)00021-3.
[27] P. Prusinkiewicz, Applications of L-systems to computer imagery BT - Graph-Grammars and Their Application to Computer Science, in: H. Ehrig, M. Nagl, G. Rozenberg, A. Rosenfeld (Eds.), Springer Berlin Heidelberg, Berlin, Heidelberg, 1987: pp. 534–548. https://doi.org/10.1007/3-540-18771-5_74.
[28] J.Z. Zhou, S. Huang, J. Sheng, J.Z. Lu, C.D. Wang, K.M. Chen, H.Y. Ruan, H.S. Chen, Effect of repeated impacts on mechanical properties and fatigue fracture morphologies of 6061–T6 aluminum subject to laser peening, Mater. Sci. Eng. A. 539 (2012) 360–368, https://doi.org/10.1016/j.msea.2012.01.125.
[29] S. Huang, J.Z. Zhou, J. Sheng, J.Z. Lu, G.F. Sun, X.K. Meng, L.D. Zuo, H.Y. Ruan, H.S. Chen, Effects of laser energy on fatigue crack growth properties of 6061–T6 aluminum alloy subjected to multiple laser peening, Eng. Fract. Mech. 99 (2013) 87–100, https://doi.org/10.1016/j.engfracmech.2013.01.011.
[30] K. Hibbitt, Sorensen, Inc. (2000), ABAQUS/standard user’s manual, 2 (2005) 14.11.
[31] C.S. Montross, T. Wei, L. Ye, G. Clark, Y.W. Mai, Laser shock processing and its effects on microstructure and properties of metal alloys: a review, Int. J. Fatigue. 24 (2002) 1021–1036, https://doi.org/10.1016/S0142-1123(02)00022-1.
[32] P. Peyre, L. Berthe, X. Scherpereel, R. Fabbro, E. Bartnicki, Experimental study of laser-driven shock waves in stainless steels, J. Appl. Phys. 84 (1998) 5985–5992, https://doi.org/10.1063/1.368894.
[33] X. Wang, J. Shi, Validation of Johnson-Cook plasticity and damage model using impact experiment, Int. J. Impact Eng. 60 (2013) 67–75, https://doi.org/10.1016/j.ijimpeng.2013.04.010.
[34] P.P.L. Matos, R.M. McMeeking, P.G. Charalambides, M.D. Drory, A method for calculating stress intensities in bimaterial fracture, Int. J. Fract. 40 (1989) 235–254, https://doi.org/10.1007/BF00963659.
[35] F. Erdogan, G.C. Sih, On the crack extension in plates under plane loading and transverse shear, J. Fluids Eng. 85 (1963) 519–525, https://doi.org/10.1115/1.3656897.
[36] A. Kotousov, P. Lazzarin, F. Berto, L.P. Pook, Three-dimensional stress states at crack tip induced by shear and anti-plane loading, Eng. Fract. Mech. 108 (2013) 65–74, https://doi.org/10.1016/j.engfracmech.2013.04.010.
[37] F. Berto, A. Kotousov, P. Lazzarin, L.P. Pook, On scale effect in plates weakened by rounded V-notches and subjected to in-plane shear loading, Int. J. Fract. 180 (2013) 111–118, https://doi.org/10.1007/s10704-012-9796-x.
[38] M. Dorman, M.B. Toparli, N. Smyth, A. Cini, M.E. Fitzpatrick, P.E. Irving, Effect of laser shock peening on residual stress and fatigue life of clad 2024 aluminium sheet containing scribe defects, Mater. Sci. Eng. A. 548 (2012) 142–151, https://doi.org/10.1016/j.msea.2012.04.002.
[39] C.H. Lloyd, I.W.M. Jeffrey, M.J.P. Mannion, The strength of lining materials under constraint, J. Oral Rehabil. 9 (1982) 435–443, https://doi.org/10.1111/j.1365-2842.1982.tb01033.x.
[40] Y.-Z. Chen, A dugdale problem for a finite internally cracked plate, Eng. Fract. Mech. 17 (1983) 579–583. https://doi.org/https://doi.org/10.1016/0013-7944(83)90117-0.
[41] G. Irwin, Plastic zone near a crack and fracture toughness, 1997.
[42] O. Plekhov, M. Paggi, O. Naimark, A. Carpinteri, A dimensional analysis interpretation to grain size and loading frequency dependencies of the Paris and Wöhler curves, Int. J. Fatigue. 33 (2011) 477–483, https://doi.org/10.1016/j.ijfatigue.2010.10.001.